Environmental Science

AIMS Environmental Science, 13(1): 99–125.
DOI: 10.3934/environsci.2026005
Received: 27 December 2025
Revised: 02 February 2026
Accepted: 13 February 2026
Published: 28 February 2026

https://www.aimspress.com/journal/environmental

Research article

Ecological synthesis, characterization and application of iron oxide of tangerine nanoparticles for arsenic removal from aqueous solutions

Hugo Sánchez-Moreno[1,*], Ingrid Haro-Chafla[2], Juan Lagua-Chango[3], Benjamín Román-Santos[4], Nelly Guananga-Díaz[5], David Espín-García[2], Lis Peñafiel- Guevara[2] and Israel Heredia-Moreno[2]

[1] Alternative Energy and Environment Research Group, Faculty of Sciences, Higher Polytechnic School of Chimborazo (ESPOCH), Panamericana Sur Km 1 ½, Chimborazo, EC060155, Ecuador; hugoj.sanchez@espoch.edu.ec
[2] Independent Research
[3] Advanced Materials Research Group, Faculty of Sciences, Higher Polytechnic School of Chimborazo (ESPOCH), Panamericana Sur Km 1 ½, Chimborazo, EC060155, Ecuador; juan.lagua@espoch.edu.ec
[4] Natural Products and Pharmacy Research Group, Faculty of Sciences, Higher Polytechnic School of Chimborazo (ESPOCH), Panamericana Sur Km 1 ½, Chimborazo, EC060155, Ecuador; benjamin.roman@espoch.edu.ec
[5] Leishmaniasis and other parasitic diseases in Ecuador Research Group, Faculty of Sciences, Higher Polytechnic School of Chimborazo (ESPOCH), Panamericana Sur Km 1 ½, Chimborazo, EC060155, Ecuador; nguananga@espoch.edu.ec

* **Correspondence:** Email: hugoj.sanchez@espoch.edu.ec; Tel.: +593987983888.

Abstract: Water pollution represents a critical global challenge affecting human health and natural ecosystems. Among the most hazardous contaminants are heavy metals, particularly arsenic (As), which is frequently detected at elevated concentrations in water bodies as a consequence of anthropogenic activities such as agriculture, mining, and metallurgical processes. In this study, magnetic iron oxide nanoparticles synthesized via a green route using tangerine (Citrus reticulata) peel extract (FeNPs-CR) were developed and evaluated for As removal from aqueous solutions. The nanoparticles were synthesized through a coprecipitation method employing 75 g of pulverized peel extract and characterized by scanning electron microscopy (SEM), FT-IR spectroscopy, UV–Vis spectroscopy, and dynamic light scattering (DLS). SEM analysis revealed quasi-spherical particles with primary sizes ranging from 70 to 300 nm, while DLS measurements indicated larger

hydrodynamic diameters due to particle agglomeration in aqueous media. Adsorption experiments were conducted using hydride generation atomic absorption spectroscopy, evaluating the effects of contact time, adsorbent dosage, pH, temperature, and initial As concentration. Removal efficiencies exceeding 99% were achieved at 20 mg/L As within 10–30 min, while concentrations of 50–120 mg/L showed removal efficiencies above 95%. Adsorption kinetics were best described by the pseudo-second-order model, indicating a physicochemical adsorption mechanism. Equilibrium data were better fitted by the Freundlich isotherm ($R^2 = 0.97$), suggesting heterogeneous multilayer adsorption, with a maximum adsorption capacity (qmax) of 227.27 mg/g. Thermodynamic analysis revealed negative Gibbs free energy ($\Delta G° = -7.66$ to -11.14 kJ/mol), confirming the spontaneous and exothermic nature of the adsorption process. Optimal performance was observed under acidic conditions (pH 1–3) and temperatures below 35 °C. These findings demonstrated that FeNPs-CR synthesized from citrus waste constitute an efficient, sustainable, and low-cost adsorbent for As removal, with promising potential for large-scale water treatment applications.

Keywords: iron oxide nanoparticles; Citrus reticulata extract; green synthesis; arsenic adsorption; adsorption isotherms; adsorption kinetics; water treatment

Highlights

- Iron oxide nanoparticles were synthesized using Citrus reticulata extract via a green synthesis approach.
- FeNPs-CR exhibited high arsenic removal efficiency (> 97%) across a wide concentration range.
- A maximum adsorption capacity (qmax) of 227.27 mg/g was achieved, indicating strong adsorption potential.
- The adsorption process reached equilibrium within 10 minutes and was governed by a combined mechanism of surface complexation and electrostatic attraction.

1. Introduction

Water contamination by As constitutes a serious global environmental and public health problem due to its high toxicity, persistence, and widespread occurrence in natural and anthropogenic water sources [1,2]. As is introduced into aquatic environments through geogenic processes, such as mineral weathering and geothermal activity, and anthropogenic sources, including mining operations, metallurgical industries, intensive agricultural practices, fossil fuel combustion, and improper disposal of industrial effluents [1]. Once released, As can persist in groundwater and surface waters, facilitating its incorporation into drinking water supplies and agricultural soils [2]. Chronic exposure to As has been associated with severe health effects, including carcinogenesis, cardiovascular and neurological disorders, hypertension, melanosis, and developmental impairments [3]. Furthermore, its accumulation in aquatic and terrestrial ecosystems reduces biodiversity, degrades soil quality, and compromises food security [4]. Consequently, the development of efficient, sustainable, and cost-effective technologies for As removal remains a critical scientific and public health priority.

Despite extensive research efforts, As remediation remains technically challenging due to its complex aqueous chemistry and stringent regulatory limits. As is considered a potent toxicant even at very low concentrations, with guideline values for drinking water established at 10 μg/L by the World

Health Organization (WHO), while concentrations in waters impacted by mining activities can reach tens to hundreds of μg/L or even mg/L levels [5,6]. The coexistence of arsenite [As(III)] and arsenate [As(V)] species further complicates treatment strategies, as As(III) is electrically neutral at near-neutral pH, more mobile, and significantly more toxic, making it difficult to remove through conventional adsorption and coagulation processes [7]. Likewise, in natural and industrial waters, the presence of competing anions such as phosphate, silicate, and carbonate can substantially reduce As removal efficiency by occupying active adsorption sites [8]. These challenges highlight the need to develop treatment technologies that combine high efficiency, selectivity, and operational robustness under environmentally relevant conditions.

Nanotechnology has enabled significant advances in environmental remediation owing to the unique physicochemical properties of nanomaterials, such as high surface area, enhanced reactivity, and tunable surface chemistry [9]. Nanomaterials can be broadly classified into naturally occurring nanoparticles and engineered nanomaterials, the latter being intentionally synthesized with controlled size, morphology, and surface functionality [10,11]. Among engineered nanomaterials, iron-based nanoparticles have attracted considerable attention for water treatment applications because of their strong affinity toward toxic metal ions, magnetic separability, chemical stability, and relatively low production cost [12].

Magnetite nanoparticles (Fe_3O_4) have gained relevance in nanotechnology due to properties such as superparamagnetism, high surface area, chemical stability, biocompatibility, high adsorption capacity, and low human toxicity, which has driven their application in environmental engineering, biomedicine, and waste treatment [12,13]. Despite these advantages, the performance of iron oxide nanoparticles can be limited by aggregation phenomena and challenges associated with post-treatment recovery [14]. To address these limitations, surface modification and stabilization strategies have been explored, including the use of environmentally friendly synthesis routes. In this context, green synthesis methods based on plant extracts have gained increasing attention as sustainable alternatives to conventional chemical approaches, as they reduce the use of hazardous reagents, lower energy consumption, and minimize secondary environmental impacts [15]. Biomolecules present in plant extracts, such as polyphenols, flavonoids, polysaccharides, and organic acids, can play multiple roles during nanoparticle formation, acting as reducing, stabilizing, and capping agents that influence particle growth and surface properties [16].

Citrus fruit residues, including tangerine peels, represent an abundant agro-industrial waste rich in phenolic compounds, pectin, cellulose, and other functional biomolecules capable of interacting with metal ions [17,18]. In Ecuador, tangerine peel derived from *Citrus reticulata* constitutes an underutilized biomass resource with high potential for waste valorization. In particular, the chemical composition of tangerine peel extract, rich in hydroxyl (–OH) and carboxyl (–COOH/–COO^-) functional groups, enables its use as a green synthesis medium by complexing Fe^{2+}/Fe^{3+} species, thereby modulating nanoparticle nucleation and growth, while the resulting organic surface coating contributes to partial colloidal stabilization through steric and electrostatic effects and provides additional active sites that enhance the adsorption capacity toward As species [19–22]. Furthermore, the incorporation of these surface functionalities into iron oxide nanoparticles reduces their surface energy, influences agglomeration processes in aqueous suspension, and provides additional active sites that promote chemical and electrostatic interactions with ionic species such as As, directly contributing to the adsorptive performance of the material [23].

Therefore, our objectives of this study are: (i) To synthesize iron oxide nanoparticles via a green route using *Citrus reticulata* peel extract; (ii) to evaluate the removal of As from aqueous solutions under different operational conditions, including contact time, pH, adsorbent dosage, initial As

concentration, and temperature; and (iii) to investigate the adsorption kinetics, equilibrium isotherms, and thermodynamic behavior of the process. The practical relevance of this work is supported by the use of water samples representative of mining-influenced environments, including those collected from the Zaruma mining district (Ecuador), where legal and informal artisanal mining activities may contribute to the mobilization of metal species into surrounding water bodies. Through this integrated approach, we aim to address challenges associated with the development of sustainable, low-cost, and magnetically recoverable nanomaterials for As remediation under environmentally relevant conditions.

2. Methodology

2.1. Reagents and materials

Ferrous chloride tetrahydrate ($FeCl_2 \cdot 4H_2O$) was obtained from LOBA Chemie Pvt. Ltd., while ferric chloride hexahydrate ($FeCl_3 \cdot 6H_2O$), sodium hydroxide (NaOH), potassium iodide, and ascorbic acid were purchased from ISOLAB Laborgeräte GmbH (Wertheim, Germany). A certified arsenic standard solution (1000 mg/L) was obtained from AccuStandard (New Haven, Connecticut, USA). All chemicals and solvents used in this study were of analytical grade and were used without further purification. Milli-Q water (resistivity: 18.2 MΩ·cm at 298 K) was used to prepare all solutions.

2.2. Obtaining and preparing the sample

Tangerine peel samples were obtained from the El Mirador nursery in the Patate canton, Ecuador (1°19′42.6″ S, 78°31′48.5″ W). Since only the peel was used, the samples were manually selected and cleaned to remove dust and plant debris that could cause cross-contamination. The sample preparation procedure consisted of washing, drying, and grinding steps. Initially, twelve tangerines were selected, washed with running tap water, and subsequently rinsed with distilled water. The fruits were then peeled, carefully removing the mesocarp and the white fibrous layer located between the peel and the pulp. The collected peels were placed in aluminum trays and air-dried at room temperature for three weeks. After air drying, the peels were transferred to an electric dehydrator and dried at 40 ℃ for 24 h. In the second and third batches, additional sets of twelve tangerine peels were dehydrated in an electric dehydrator for two consecutive days at a constant temperature of 30 ℃. This temperature was selected to simulate maximum ambient conditions and to preserve the antioxidant properties of the peels. Finally, the dried peels were crushed using a mortar and pestle and further pulverized into a fine powder, preparing the material for subsequent use [24,25].

2.3. Obtaining the aqueous extract of Citrus Reticulata

To prepare the extract from dried and pulverized tangerine peels (*Citrus reticulata*), an experimental protocol adapted from the literature was followed [26]. A total of 500 mL of distilled water was added to a 600 mL flask and heated on a hot plate until reaching 80°C. Subsequently, 25 g of powdered tangerine peel were added to the flask. The mixture was maintained at 80°C under continuous boiling for 15 min. After heating, the flask was removed from the hot plate and allowed to cool to room temperature. The resulting solution was filtered using filter paper with a pore size of 0.45 μm, and the obtained extract was transferred to a suitable container for storage. The same procedure was repeated using increased amounts of tangerine peel powder (50 g and 75 g), employing identical experimental conditions. The resulting extracts were labeled as M1, M2, and M3, corresponding to

peel masses of 25 g, 50 g, and 75 g, respectively.

2.4. Synthesis of nanoparticles

The coprecipitation method was used to synthesize particles, including two iron salts, iron chloride (II) tetrahydrate ($FeCl_2 \cdot 4H2O$), and iron chloride (III) hexahydrate ($FeCl3 \cdot H2O$), in proportions of 0.47 g and 1.14 g, respectively, dissolved in 100 ml of deionized water. Of this solution, 100 ml was taken, and 0.4 ml of the previously obtained mandarin peel extract was slowly added and mixed, ensuring a homogeneous mixture. To adjust the pH, a 1 M sodium hydroxide (NaOH) solution was used, adding it drop by drop until a pH of 10 was reached, maintaining constant stirring for 20 min. The resulting particles were allowed to precipitate and were filtered and dried in an oven at 60°C for 24 h. The same procedure was carried out for the other 2 extracts: 50 g and 75 g of pulverized tangerine peel. Samples synthesized from the extracts with a quantity of tangerine peel powder of 25 g, 50 g, and 75 g were named N1, N2, and N3, respectively.

2.5. Nanoparticle characterization

The coprecipitation method was employed for nanoparticle synthesis. Two iron salts, $FeCl_2 \cdot 4H_2O$ and $FeCl_3 \cdot 6H_2O$, were used in amounts of 0.47 g and 1.14 g, respectively, and dissolved in 100 mL of deionized water. Subsequently, 0.4 mL of the previously obtained tangerine peel extract was slowly added to the solution under continuous stirring to ensure homogeneity. The pH of the mixture was adjusted to 10 by the dropwise addition of 1 M NaOH, and stirring was maintained for 20 min. The resulting particles were allowed to precipitate, then separated by filtration and dried in an oven at 60 ℃ for 24 h. The same synthesis procedure was repeated using extracts prepared from 50 g and 75 g of pulverized tangerine peel. The samples synthesized using extracts obtained from 25 g, 50 g, and 75 g of tangerine peel powder were designated N1, N2, and N3, respectively.

2.6. Atomic absorption spectroscopy

For the quantitative determination of As, hydride generation atomic absorption spectroscopy (HG-AAS) was employed. This technique was selected due to its high sensitivity and its ability to minimize matrix interferences, which are common in arsenic analysis [27]. The procedure involved the addition of a reducing agent, sodium borohydride ($NaBH_4$), to the previously acidified sample. This reaction converted the arsenic present in the sample into a volatile gaseous species, arsine (AsH_3), which was subsequently detected by atomic absorption spectroscopy (AAS).

2.7. Viability of the particle as a retainer of As in water

To evaluate the arsenic retention capacity, a certified As(III) standard solution (1000 mg/L) was used. From this stock solution, a working solution of 1.0 mg/L was prepared and subsequently used to generate the different test solutions for the adsorption assays. These solutions were brought into contact with FeNPs-CR under the established experimental conditions. After equilibrium was reached, the suspensions were filtered, and the residual arsenic concentration was determined by atomic absorption spectrometry. The percentage of arsenic adsorption by FeNPs-CR was then calculated based on the initial and final concentrations.

2.7.1. Effect of contact time

To determine the equilibrium time of the synthesized particles, 0.1 g of FeNPs-CR was added to 200 mL of an aqueous solution containing 1000 μg/L of As. The suspension was initially subjected to ultrasonic agitation for 10 s and subsequently maintained under intermittent mechanical stirring for 4 h at a controlled temperature of 27 ℃. During the experiment, 1 mL aliquots of the liquid phase were collected at 5 min intervals during the first 30 min and then at hourly intervals thereafter. Each aliquot was diluted to a final volume of 10.0 mL, and the arsenic concentration was determined by atomic absorption spectroscopy.

2.7.2. Effect of FeNPs-CR mass as an adsorbent

To determine the optimal adsorbent dosage for arsenic retention, five samples were prepared using different masses of FeNPs-CR: 0.025, 0.05, 0.1, 0.3, and 0.5 g. Each adsorbent mass was added separately to 200 mL of an aqueous solution containing 1000 μg/L of As(III) at a constant temperature of 27 ℃. The suspensions were stirred at 200 rpm until adsorption equilibrium was reached. Subsequently, a 1.0 mL aliquot of the solution was carefully withdrawn and diluted to a final volume of 10.0 mL with deionized water to adjust the arsenic concentration to the analytical detection range. The residual arsenic concentration in each diluted aliquot was then quantified using AAS.

2.7.3. Effect of pollutant concentration (As)

To evaluate the effect of contaminant concentration on the adsorption process, a series of 200 mL aqueous solutions with initial arsenic concentrations ranging from 1 to 120 mg/L were prepared. To each solution, 0.1 g of FeNPs-CR was added, and the suspensions were stirred at 200 rpm at room temperature for 15 min. After adsorption, 1.0 mL aliquots were collected from each solution and diluted to a final volume of 10.0 mL. The residual arsenic concentration was then determined using atomic absorption spectroscopy. All experiments were performed in duplicate to ensure data reproducibility.

2.7.4. Effect of pH on retention

Aqueous solutions of 200 mL were prepared at different pH values (1.0, 2.0, 4.0, 6.0, and 7.0), each containing an initial arsenic concentration of 10 mg/L. The pH was adjusted using 0.1 M HCl and 0.1 M NaOH solutions. After reaching the desired pH, 0.1 g of FeNPs-CR was added to each solution, and the suspensions were stirred at 200 rpm at room temperature until adsorption equilibrium was achieved. Subsequently, 1.0 mL aliquots were withdrawn and diluted to a final volume of 10.0 mL. The residual arsenic concentration was then determined using AAS.

2.7.5. Influence of temperature

The effect of temperature on arsenic adsorption was evaluated at controlled temperatures of 27, 35, and 45 ℃. Aqueous solutions of 200 mL with an initial arsenic concentration of 10.0 mg/L were prepared. To each solution, 0.1 g of FeNPs-CR was added without pH adjustment, and the suspensions were stirred at a constant speed of 200 rpm. Samples were collected at contact times of 1, 2, 3, 5, 8,

10, 15, 20, and 30 min. Subsequently, 1.0 mL aliquots of the liquid phase were withdrawn and diluted to a final volume of 10.0 mL. The residual arsenic concentration was then determined using AAS.

2.8. Adsorption isotherm

Two adsorption isotherm models were applied to analyze the experimental data obtained in this study, namely the Langmuir and Freundlich isotherms. The maximum adsorption capacity was determined by maintaining a constant amount of adsorbent (FeNPs-CR) while varying the initial concentration of arsenic in the aqueous solution. For this purpose, the equilibrium concentration (Ce, mg/L) was plotted against the amount of arsenic adsorbed per unit mass of adsorbent (qe, mg/g), according to Eq (1). In this equation, Ci and Cf represent the initial and final arsenic concentrations in solution, respectively (mg/L), W corresponds to the mass of the adsorbent (g), and V denotes the volume of the test solution (L).

$$q = \frac{Ci - Cf}{W} \times V \tag{1}$$

The linear form of the Langmuir isotherm model is expressed by Eq (2) [28]:

$$Langmuir: \quad \frac{Ce}{q} = \frac{1}{q_m \times KL} + \frac{Ce}{q_m} \tag{2}$$

where qm represents the maximum adsorption capacity (mg/g) and KL is the Langmuir equilibrium constant (L/mg).

One of the key parameters of the Langmuir isotherm is the dimensionless separation factor (RL), which is expressed by Eq (3):

$$RL = \frac{1}{1 + KL \times Co} \tag{3}$$

where Co (mg/L) is the initial adsorbate concentration. Values of RL between 0 and 1 indicate favorable adsorption.

The Freundlich isotherm describes heterogeneous and multilayer adsorption on the surface of the adsorbent and is expressed as follows:

$$Freundlich: \quad Log\ q = Log\ Kf + \frac{1}{n} LogCe \tag{4}$$

where Kf indicates the Freundlich constant expressed in (mg $^{1-1/n}$ g $^{-1}$ L $^{1/n}$) related to the adsorption capacity, while 1/n (dimensionless) is the adsorption intensity [29].

2.9. Thermodynamic study

The calculation of the standard change in Gibbs free energy associated with the adsorption process was performed using the equation:

$$\Delta G^0 = -RT \ln K_c \tag{5}$$

where R is the universal gas constant (8.314 J mol^{-1} K^{-1}), T is the absolute temperature (K), and Kc is the adsorption equilibrium constant.

$$Kc = \frac{Co - Ce}{Ce} \tag{6}$$

where Co is the initial concentration of arsenic and Ce is the equilibrium concentration in solution,

both expressed in mg L^{-1}. The standard enthalpy (ΔH°) and entropy (ΔS°) changes were determined from the slope and intercept of the linear plot of ln Kc versus 1/T.

3. Results

3.1. Obtaining aqueous extract from E. grandis

The aqueous extract exhibited a slightly yellowish coloration. Its chemical composition was analyzed by FTIR spectroscopy, as shown in Figure 1, where M1, M2, and M3 correspond to extracts obtained from 25 g, 50 g, and 75 g of tangerine peel powder, respectively. All three samples display similar FTIR spectra with characteristic absorption bands associated with typical citrus-derived compounds. A broad absorption band observed between 3320.82 and 3332.39 cm^{-1} is attributed to C–H stretching vibrations associated with alkene groups. Additionally, bands in the range of 1639.20–1649.05 cm^{-1} may be assigned to N–O stretching vibrations of functional groups present in the citrus extract. The absorption region between 2129.02 and 2144.45 cm^{-1} suggests the presence of functional groups related to ketones, aldehydes, or pectin-derived compounds [30].

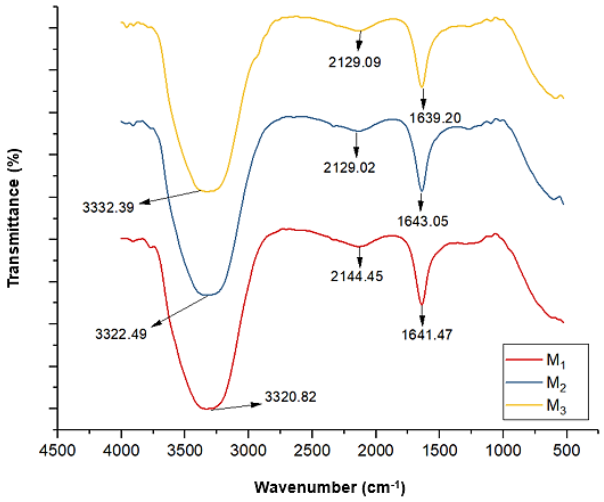

Figure 1. Infrared spectrum of mandarin extract (Citrus Reticulata). The concentrations of pulverized tangerine peel were varied: 25, 50, and 75 g. Test conditions: V=500 mL of deionized water; T=80 °C; and t=15 min.

3.2. Synthesis of particles

The concentration of NaOH, the volume of tangerine peel extract, and the synthesis temperature were had a significant influence on the formation of iron oxide nanoparticles (Fe_3O_4). The tangerine peel extract acts as a reducing and stabilizing agent during nanoparticle synthesis. Sodium hydroxide (NaOH) was used to adjust the pH and promote particle precipitation. Adjusting the pH to approximately 10 favored the acquisition of a negative surface charge by FeNPs-CR, generating electrostatic repulsion between particles. This repulsion enhanced dispersion in the aqueous medium and reduces particle agglomeration. The synthesis temperature was maintained at ambient conditions to prevent oxidation of the iron species and to avoid thermal degradation of the organic compounds present in the natural extract [31].

3.3. Characterization of particles

The characterization of FeNPs-CR was carried out using SEM and spectroscopic techniques. SEM analysis was performed using a Tescan Vega 3 microscope. UV–Vis spectroscopy and FTIR spectroscopy were employed to investigate the optical properties and surface functional groups of the synthesized nanoparticles. FTIR spectra were recorded using a CE 3000 Series spectrometer.

3.3.1. FT-IR Spectroscopy

FTIR was used to analyze the functional groups present on the surface of FeNPs-CR and to assess the contribution of biomolecular species involved in nanoparticle coating and stabilization. Figure 2 shows the FTIR spectra of FeNPs-CR samples N1, N2, and N3, synthesized using extracts M1, M2, and M3, respectively. In all cases, a constant extract volume of 0.4 mL was employed during synthesis.

The FTIR spectra of FeNPs-CR exhibited characteristic bands at 1600.62 cm^{-1} and 3328.53 cm^{-1}, which were associated with vibrational modes of water molecules adsorbed on the nanoparticle surface, a feature commonly reported for magnetite-based materials. In addition, absorption bands at 524.54 and 567 cm^{-1} corresponded to Fe–O bond vibrations, confirming the formation of iron oxide nanoparticles [32].

The band observed around 3328.53 cm^{-1} was attributed to O–H stretching vibrations. In this study, the broadening and decrease in transmittance intensity of the bands at 3328.53 and 1600.62 cm^{-1} indicated the presence of surface functional groups derived from the tangerine peel extract. These groups are characteristic of citrus-based biomolecules and contribute to the stabilization of FeNPs-CR [33,34].

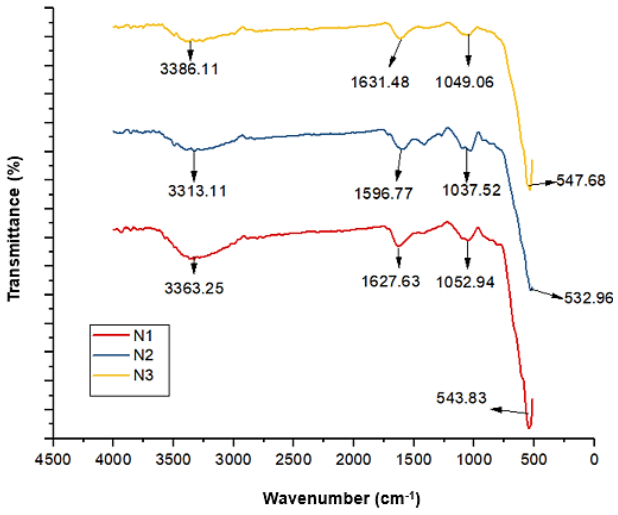

Figure 2. FT-IR spectrum of FeNPs-CR N1, N2, and N3. The amount of powdered tangerine peel extracts was varied: 25, 50, and 75g. Test conditions: 150 rpm; V=500 mL of deionized water; T=27 °C; and t=55 min.

Considering the magnetic response of the particles and the results obtained from SEM analysis, sample N3 was selected for subsequent experiments. Accordingly, this sample was used in all arsenic removal studies.

3.3.2. Scanning Electron Microscopy (SEM)

SEM was used to determine the size and morphology of FeNPs-CR. Among the three samples analyzed, N3 exhibited the most representative size and morphology characteristic of this type of nanomaterial. Based on the SEM analysis, the particle sizes of FeNPs-CR ranged from 70 to 300 nm, although particles larger than 100 nm were also observed. The presence of larger particles could be attributed to the organic components of the tangerine peel extract, such as sugars, as well as to the intrinsic tendency of this type of nanomaterial to undergo agglomeration [35]. The observed morphology corresponded to a reverse spinel structure with a non-homogeneous crystalline arrangement, and the particles appeared irregularly distributed on the sample holder. Figure 3 presents the SEM micrographs and size distribution of FeNPs-CR samples N1, N2, and N3. All samples were analyzed at different accelerating voltages and magnifications to ensure representative morphological characterization. The results obtained in this study are consistent with previous reports on FeNPs-CR synthesized using tangerine peel extracts [36,37].

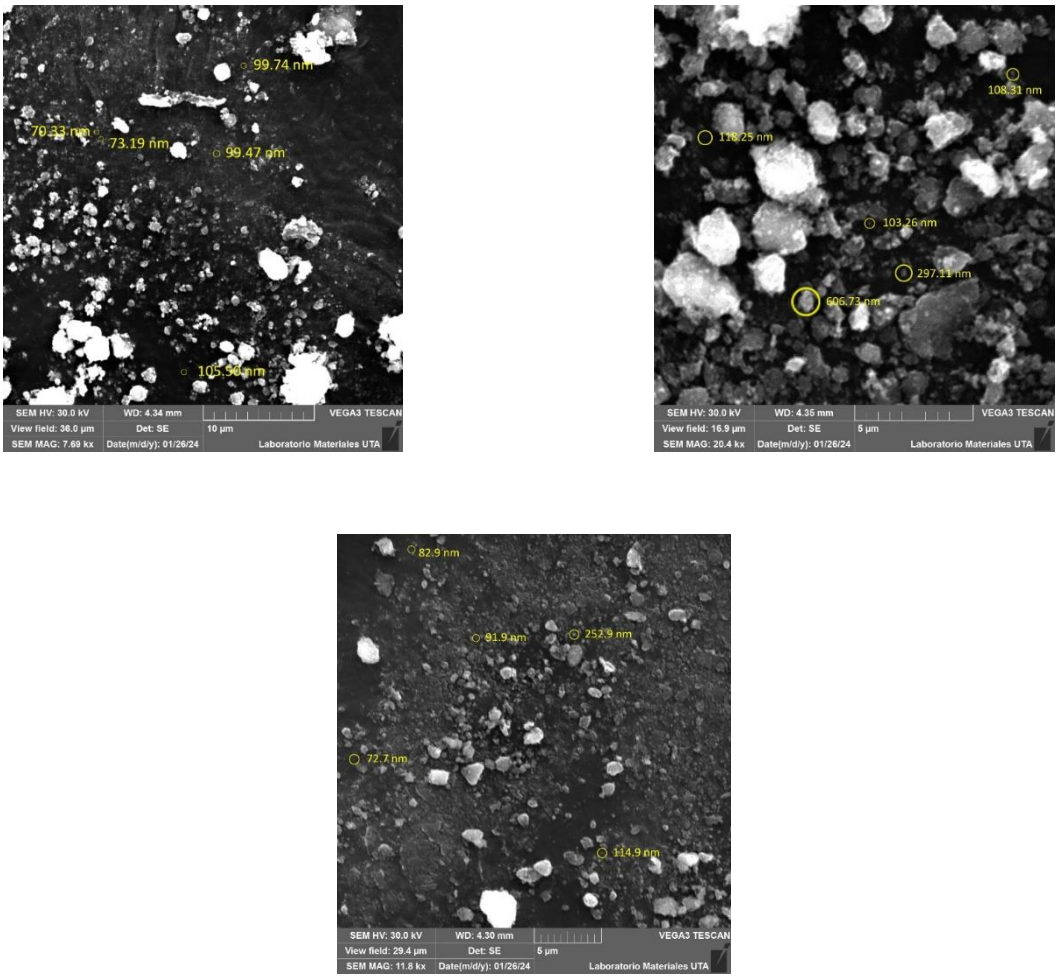

Figure 3. SEM micrograph of FeNPs-CR.

3.3.3. UV-Vis spectroscopy

The UV–Vis spectra (Figure 4) showed characteristic absorption bands with average wavelengths at 263 and 290 nm. These absorption features were attributed to electronic transitions associated with the intrinsic bandgap of FeNPs-CR. The absorption process corresponded to the excitation of electrons from the valence band to the conduction band. The energy associated with these electronic transitions could be described by the quantized energy equation, where h is Planck's constant, c is the speed of light, and λ is the wavelength of the absorbed radiation.

$$E = \frac{hc}{\lambda}\lambda \tag{7}$$

The estimated bandgap energy was approximately 4.72 eV, which is consistent with values reported in the literature for similar materials. This indicated that FeNPs-CR absorb light as a result of electronic transitions between discrete energy levels. These transitions involve changes in the electronic configuration of iron and oxygen atoms, leading to the absorption of photons at specific wavelengths [38].

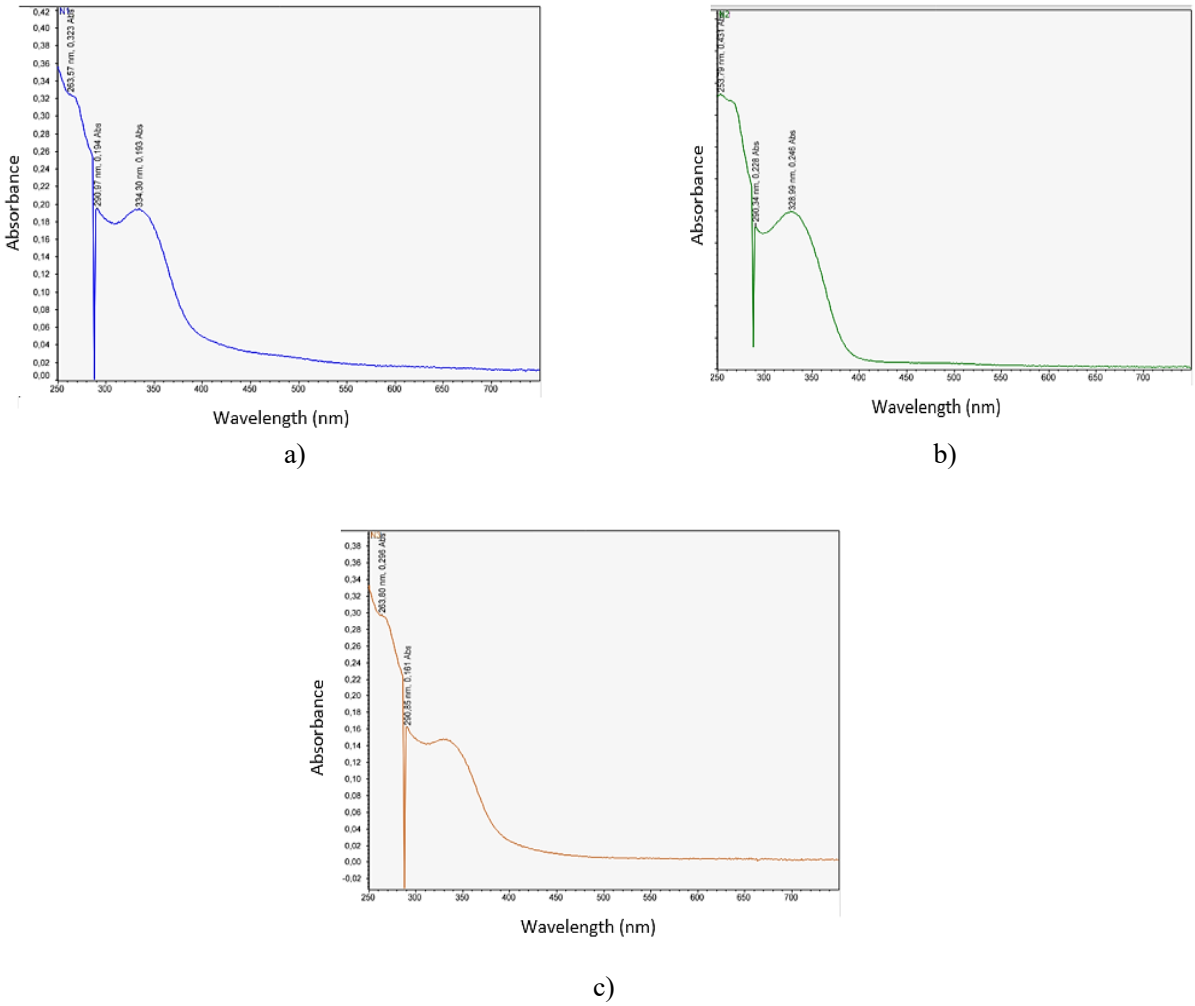

Figure 4. UV–Vis spectra of FeNPs-CR samples synthesized using different amounts of *Citrus reticulata* (tangerine) peel extract: (a) 25 g, (b) 50 g, and (c) 75 g.

3.3.4. DLS (dynamic light scattering) analysis

The laser granulometry analysis was carried out in the Department of Extractive Metallurgy at the National Polytechnic School using a Laser Scattering Particle Size Distribution Analyzer LA-950V2 (HORIBA). The measurements were interpreted using Mie theory, which describes the scattering of electromagnetic waves by spherical particles, employing a refractive index of 2.42 for magnetite.

The DLS measurements revealed a broad hydrodynamic size distribution ranging from 0.1 to 17.4 μm (Figure 5), indicating the presence of aggregated particles and agglomerates in aqueous suspension rather than isolated primary nanoparticles. In systems synthesized via green routes, organic ligands present in the plant extract can significantly increase the hydrodynamic diameter measured by DLS, as the organic coating and its solvation layer contribute to the effective size of the nanoparticles in suspension [39]. In this context, magnetic dipole–dipole interactions inherent to magnetite, together with Lifshitz–van der Waals forces and the absence of synthetic surfactants, may favor the formation of reversible agglomerates in aqueous media [40,41]. Similar hydrodynamic size distributions (0.1–0.2 μm) have been reported for magnetite-based systems analyzed by DLS [42].

It is important to emphasize that DLS provides the hydrodynamic diameter of particle aggregates dispersed in liquid media, whereas SEM analysis reflects the primary particle size in the dry state. Therefore, the larger sizes detected by DLS do not contradict the nanoscale dimensions observed by SEM, but rather confirm the tendency of FeNPs-CR to form agglomerates in aqueous environments [43].

Although a more homogeneous dispersion and smaller hydrodynamic sizes (< 0.1 μm) could further enhance adsorption performance, the high As removal efficiencies obtained in this study demonstrated that the aggregated FeNPs-CR remained highly effective under the evaluated experimental conditions. Nevertheless, future optimization of synthesis parameters could be explored to improve size homogeneity and dispersion stability.

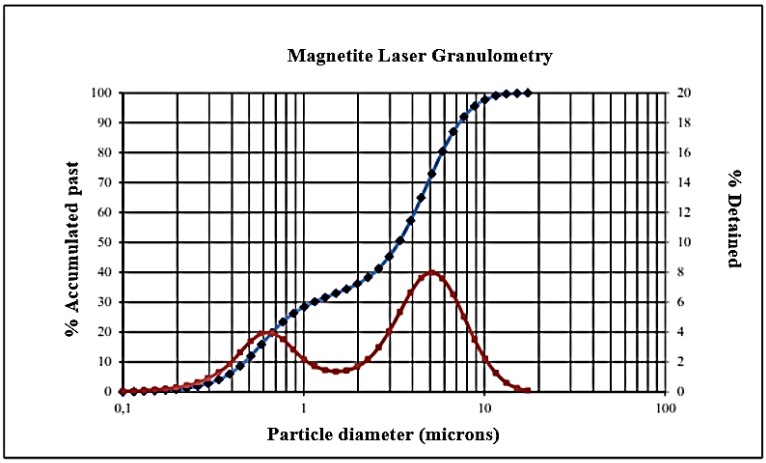

Figure 5. FeNPs-CR laser granulometry.

3.4. Equilibrium time, dosage, and effect of pH on retention

3.4.1. Effect of contact time

Following the established methodology, adsorption experiments were carried out using FeNPs-CR under the following conditions: initial As concentration of 1 mg/L, adsorbent dosage of 0.1 g, pH 2.76,

and varying contact times. The results revealed high arsenic removal efficiencies for all samples. Specifically, the maximum removal efficiencies were 98.11% for N1 at 25 min, 98.41% for N2 at 30 min, and 98.90% for N3 at 10 min, as shown in Figure 6.

These results were used to determine the appropriate contact time for subsequent adsorption experiments. It was observed that increasing the contact time beyond the optimal value did not improve adsorption performance; instead, a decrease in arsenic removal efficiency was detected at longer contact times. Furthermore, within the first 5 min of contact, FeNPs-CR achieved arsenic removal levels ranging from approximately 90% to 97%, indicating rapid adsorption kinetics and a strong affinity between arsenic species and the adsorbent surface.

Based on these findings, FeNPs-CR demonstrated a high arsenic removal capacity within a short contact time, confirming their suitability for further studies on heavy metal remediation. Considering the adsorption performance and the morphological and structural characteristics of FeNPs-CR, an optimal contact time between 10 and 30 min was established. For sample N3, which was selected for subsequent experiments, the optimal contact time was 10 min. This selection was supported by the particle size distribution of N3, which provided a relatively large surface area and high removal efficiency, validating its effectiveness for arsenic removal under the studied conditions.

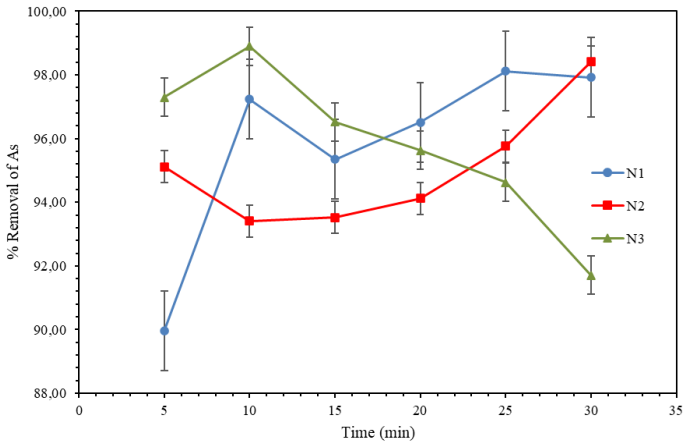

Figure 6. Contact time evaluation. As(III) removal capacity of N1, N2, and N3 nanoparticles. Test conditions: 200 rpm; V=100 mL; T=27 °C; and t=35 min.

3.4.2. Effect of FeNPs-CR mass as an adsorbent

For this analysis, a solution volume of 100 mL with an initial As concentration of 1 mg/L and a pH of 2.26 was used. Different masses of FeNPs-CR were evaluated, specifically 0.025, 0.05, 0.1, 0.3, and 0.5 g. Figure 7 illustrates the corresponding arsenic removal efficiencies obtained for each adsorbent dosage. The results showed that, at a contact time of 10 min, the highest removal efficiency (90.92%) was achieved using 0.1 g of FeNPs-CR, whereas the lowest removal efficiency (20.23%) was observed with 0.025 g.

Optimizing the adsorbent dosage is a critical factor in adsorption processes, particularly in systems that employ magnetic separation for particle recovery. Using lower amounts of adsorbent facilitates magnetic separation by reducing the required magnetic energy and preventing saturation of the recovery system. In addition, lower particle concentrations help minimize agglomeration, which commonly occurs at higher dosages due to van der Waals forces and magnetic interactions in FeNPs-CR.

Particle agglomeration reduces the effective surface area available for adsorption and consequently decreases adsorption efficiency.

At lower adsorbent concentrations, arsenic transport to active surface sites may be more efficient due to reduced competition for adsorption sites and improved dispersion in the solution. Furthermore, the use of optimized adsorbent dosages can prevent undesirable effects such as particle–particle interactions, local pH variations, or partial deactivation of FeNPs-CR induced by excessive solid loading.

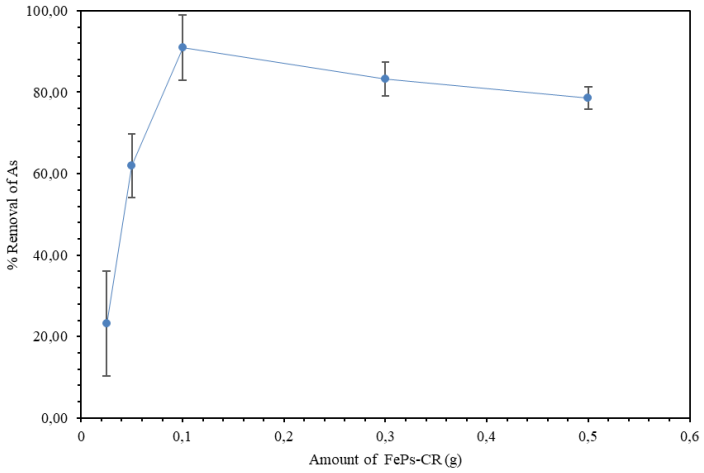

Figure 7. Effect of the mass of FeNPs-CR varying the amount of N3. Test conditions: 200 rpm; V=100 mL; T=27 °C; and t=10 min.

3.4.3. Effect of pH on adsorbent capacity

Figure 8 presents the results obtained from the evaluation of pH on arsenic removal. At acidic pH values of 1 and 3, removal efficiencies higher than 98% were achieved, with a slight increasing trend as contact time progressed. At pH 5, which is also considered acidic, greater variability in removal efficiency was observed, with values ranging from approximately 96% to a maximum of 97.2%. At neutral pH (pH 7), removal efficiencies above 98% were observed within the first 3 min; however, at longer contact times, the removal efficiency did not exceed 97%. These results indicated that FeNPs-CR exhibited higher arsenic removal efficiency under acidic conditions, which is consistent with findings reported by other authors [44,45].

Under acidic conditions, the surface of FeNPs-CR was predominantly protonated, resulting in a positively charged surface that favors the electrostatic attraction of anionic arsenic species. In contrast, at higher pH values, surface deprotonation led to a negatively charged surface, which could reduce adsorption efficiency due to electrostatic repulsion. Between these conditions, there existed an acidic pH range in which adsorption efficiency was maximized, likely due to optimal electrostatic interactions.

Overall, FeNPs-CR exhibited arsenic removal efficiencies higher than 95% in aqueous systems under acidic and neutral pH conditions.

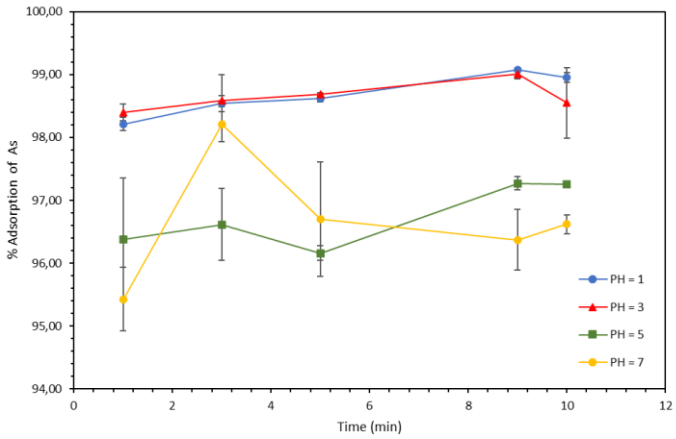

Figure 8. Effect of pH on the As Removal Process Test conditions: 200 rpm; V=100 mL; T=27 °C; t=10 min; and 0.1 g FeNPs-CR.

The point of zero charge (PZC) analysis (Figure 9) indicated that the adsorption capacity of arsenic increased as the pH approached 5.5. At low pH values, FeNPs-CR surfaces were protonated, generating a positive surface charge that enhanced the attraction of arsenic anions. Maximum adsorption was observed at approximately pH 4. At pH values above 5.5, surface deprotonation resulted in a negatively charged surface, leading to a decrease in arsenic adsorption due to electrostatic repulsion. These findings confirmed that acidic conditions are more favorable for arsenic adsorption onto FeNPs-CR. In addition, the results suggested that adsorption is not governed exclusively by electrostatic interactions related to the PZC, but also involves physical attraction mechanisms associated with the magnetic properties of the particles [46].

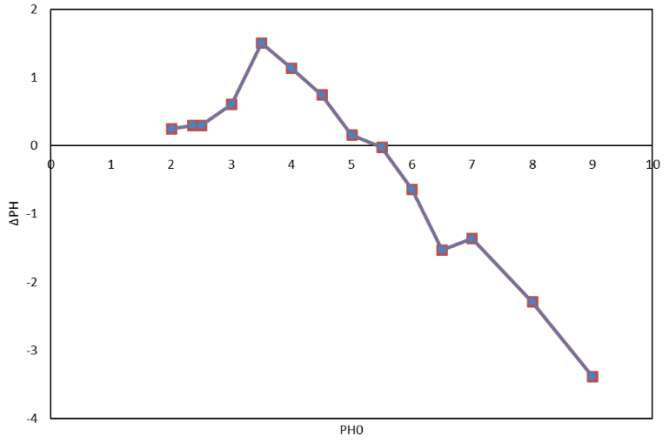

Figure 9. Determination of pH PZC in the FeNPs-CR. samples**.** Test conditions: 200 rpm; V=10 mL; T=27 °C; and 0.1 g FeNPs-CR.

3.4.4. Effect of pollutant concentration (As)

Figure 10 shows that, regardless of the initial As concentration (1, 10, and 20 mg/L), all adsorption profiles exhibit a similar initial trend, characterized by a rapid increase in removal efficiency during

the first minutes of contact. This behavior indicated fast adsorption kinetics and a strong affinity between As species and the FeNPs-CR surface. Subsequently, the adsorption curves tended to stabilize, indicating that the system reached a near-equilibrium state within a short contact time.

Under these near-equilibrium conditions, when removal efficiencies exceeded 95%, minor variations in the measured values may have become apparent. These variations could be associated with the rapid saturation of active sites, dynamic surface redistribution processes, and analytical variability inherent to the measurement of very low residual As concentrations, rather than with real changes in the intrinsic efficiency of the adsorption process. As a result, the adsorption profiles flattened after the initial uptake stage, masking a defined kinetic trend once equilibrium was reached.

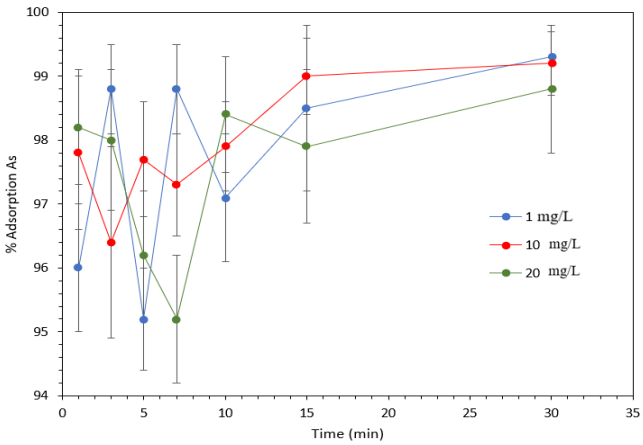

Figure 10. Effect of As concentration (mg/L). Test conditions: 200 rpm; V=100 mL; T=27 °C; and Time = 1–30 min.

Figure 11 shows the effect of the initial As concentration on removal efficiency at a fixed contact time of 10 min, corresponding to the equilibrium time determined from kinetic experiments. The removal efficiency increased from 97.12% at 1 mg/L to a maximum value of 99.33% at 20 mg/L. At higher concentrations (50–120 mg/L), the removal efficiency remained consistently high (> 97%) but did not follow a strictly monotonic pattern; for example, the efficiency at 50 mg/L was higher than those observed at 1, 10, 80, and 120 mg/L, although it remained below the maximum achieved at 20 mg/L.

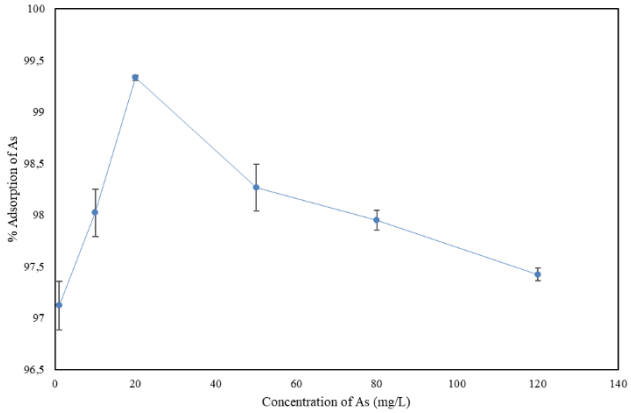

Figure 11. Effect of As concentration in time 10 min. Test conditions: 200 rpm; V=100 mL; T=27 °C; and t=10 min.

The highest removal efficiency observed at 20 mg/L indicated an optimal balance between As availability in solution and the density of active adsorption sites on the FeNPs-CR surface. At lower concentrations (1–10 mg/L), although high removal efficiencies were achieved, the reduced As availability and the higher relative impact of analytical variability at very low residual concentrations may have resulted in slightly lower apparent removal percentages. At elevated concentrations, the adsorption performance remained high, reflecting the strong affinity of FeNPs-CR toward As under the evaluated equilibrium conditions.

For As concentrations between 50 and 120 mg/L, only duplicate measurements were performed. This decision was based on the analytical limitations of the HG-AAS technique when operating near its detection limits at high removal levels, as well as on the limited availability of As standard solutions required for calibration. Under these conditions, duplicate measurements were considered sufficient to ensure data reliability and to evaluate concentration-dependent trends.

Additionally, at higher As concentrations, changes in the physicochemical behavior of the system may have occurred due to increased ionic strength and local variations in solution chemistry. These effects can influence interparticle interactions, potentially inducing partial dispersion or reversible agglomeration phenomena of the FeNPs-CR in aqueous suspension [47].

3.4.5. Effect of temperature

The effect of temperature on arsenic adsorption was evaluated by analyzing changes in the adsorption performance of FeNPs-CR as a function of temperature. An increase in temperature resulted in a decrease in adsorption efficiency, indicating that the process is exothermic. In exothermic adsorption systems, the equilibrium between adsorbed and desorbed arsenic species shifts toward desorption as thermal energy increases.

As shown in Figure 12, at 27 ℃, the initial arsenic removal efficiencies ranged from 96% to 99% within the first 5 min and stabilized at values above 97% between 20 and 30 min. At 35 ℃, the initial removal efficiencies decreased to approximately 90%–92%, reaching stabilization at around 97% only after longer contact times. In contrast, at 45 ℃, although removal efficiencies of 96%–97% were observed within the first 1–5 min, a significant decrease was detected at longer contact times, with removal efficiencies dropping to 89.7% after 30 min.

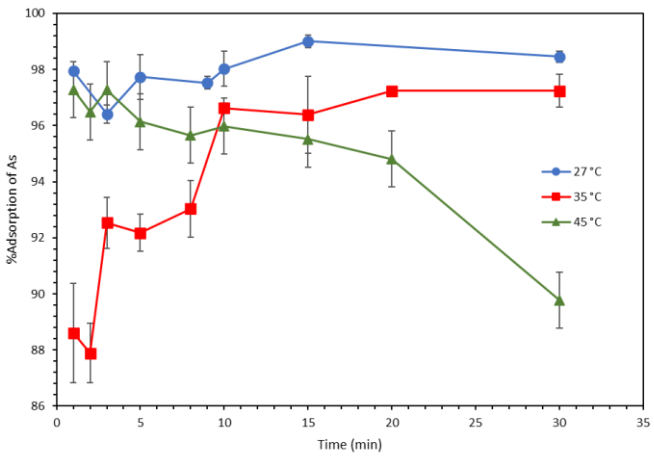

Figure 12. Effect of temperature. Test conditions: 200 rpm; V=100 mL; T=27 °C; and t=30 min.

These results demonstrated an inverse relationship between temperature and adsorption efficiency, confirming that higher temperatures reduced arsenic removal by FeNPs-CR. This behavior could be attributed to the weakening of interactions between arsenic species and the adsorbent surface at elevated temperatures. In exothermic processes, interactions such as van der Waals forces, hydrogen bonding, and weak ionic interactions become less effective as thermal energy increases, facilitating desorption. Additionally, increased atomic and molecular vibrations at higher temperatures reduce the stability of both physical and chemical interactions between FeNPs-CR and arsenic species.

These findings are consistent with other studies, such as that reported by Pillai et al. (2020), who investigated arsenic removal using iron oxide nanoparticles modified with rice husk. Their results showed enhanced arsenic removal at lower temperatures and a gradual decrease in adsorption efficiency with increasing temperature. This behavior was attributed to increased randomness and mobility of arsenic ions at higher temperatures, which hinders stable adsorption [32].

3.5. Adsorption isotherms

The adsorption capacity of FeNPs-CR was evaluated using initial arsenic concentrations of 1, 10, 20, 50, 80, and 120 mg/L. The equilibrium data were analyzed using the Langmuir and Freundlich isotherm models under identical experimental conditions. The linearized forms of the Langmuir (Eq (2)) and Freundlich (Eq (4)) models were applied to interpret the adsorption behavior. The adsorption capacity is influenced by several physical parameters, including the particle size of FeNPs-CR (70–300 nm), their spatial distribution, magnetic nature, contact time, and temperature. The combined effect of these factors contributes to the observed adsorption performance of FeNPs-CR. The use of isotherm models enables the evaluation of the adsorption mechanism and the interaction between arsenic species and the adsorbent surface [48].

The Langmuir (Figure 13) and Freundlich (Figure 14) models were fitted using equilibrium data obtained at 27°C and 200 rpm over a range of arsenic concentrations. The coefficient of determination (R^2) was used to assess the goodness of fit of each model. The corresponding isotherm parameters for different arsenic concentrations are presented in Table 1. In this study, the Freundlich model exhibited a significantly higher R^2 value (0.97) than the Langmuir model (0.46), indicating that the adsorption of arsenic onto FeNPs-CR is better described by the Freundlich isotherm [49].

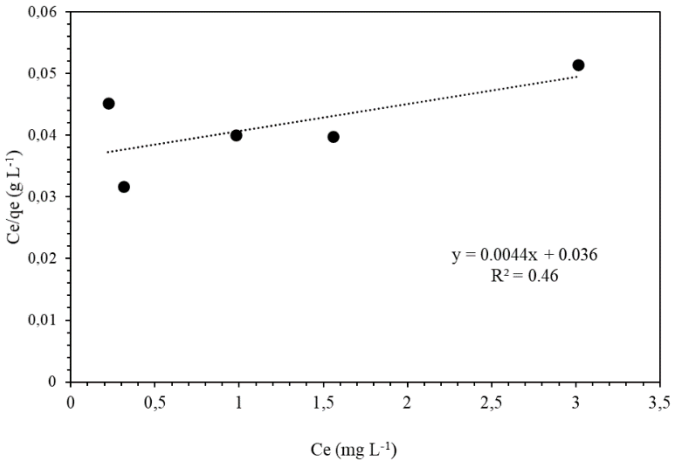

Figure 13. Langmuir isotherm for different concentrations of As.

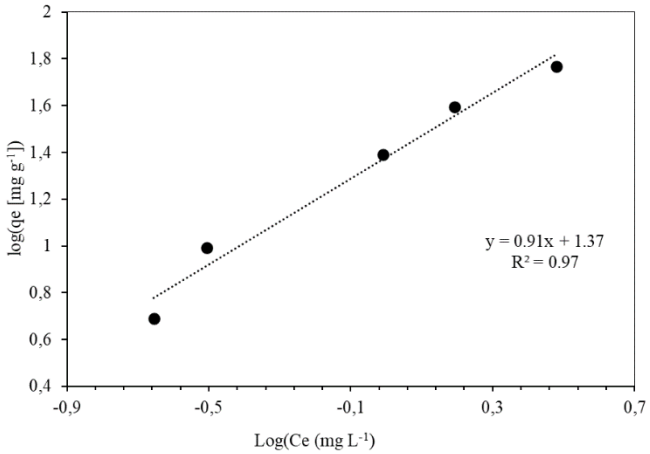

Figure 14. Freundlich isotherm for different concentrations of As.

Table 1. Parameters of Isothermal models for different concentrations of As.

Adsorption Isotherm Model	Parameters	Value with FeNPs-CR
Langmuir isotherm	qmax (mg/g)	227.27
	R^2	0.46
	KL (mg/g)	0.12
Freundlich isotherm	1/n	1.089
	Kf (mg/g)	23.87
	R^2	0.97

The better performance of the Freundlich model suggested that the surface of FeNPs-CR is heterogeneous, as confirmed by the characterization results. Additionally, the adsorption process likely involves multilayer formation and relatively weak interactions between the adsorbent and arsenic species, with incomplete surface saturation under the studied conditions [50,51].

3.6. Adsorption kinetics

Kinetic adsorption experiments were conducted independently from the factorial adsorption tests. Specifically, arsenic concentrations of 1, 10, and 20 mg/L were selected for the kinetic analysis to evaluate the adsorption mechanism under controlled conditions. These concentrations represented low, intermediate, and relatively high arsenic levels, respectively, and the resulting datasets were used exclusively for kinetic modeling.

The kinetic study was carried out at arsenic concentrations of 1, 10, and 20 mg/L. The experimental data were fitted to the pseudo-first-order and pseudo-second-order kinetic models, as shown in Figures 15 and 16. Although both models exhibited apparent linearity, the pseudo-first-order model was discarded because the calculated qe values were significantly lower than the experimentally obtained values, indicating a poorer description of the adsorption process.

In contrast, the pseudo-second-order model provided the best fit to the experimental data, as confirmed by the high regression coefficients (R^2 = 1.00 for 20 mg/L, 0.99 for 10 mg/L, and 0.9999 for 1 mg/L) and by qe values that closely matched the experimental results. These results indicated

that the rate-limiting step is governed by surface adsorption and that arsenic removal occurs predominantly through physicochemical interactions between arsenic species and the FeNPs-CR surface, which agrees with other reports [52,53].

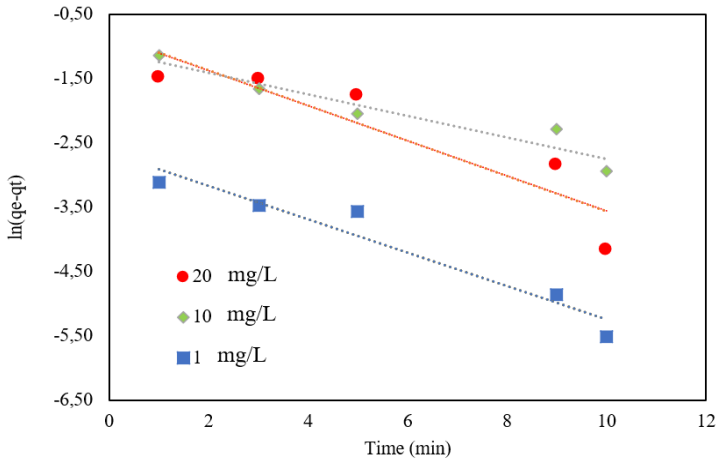

Figure 15. Linearity of the pseudo-first-order kinetic model. Adsorption experiments of As at 1, 10, and 20 mg/L using FeNPs-CR.

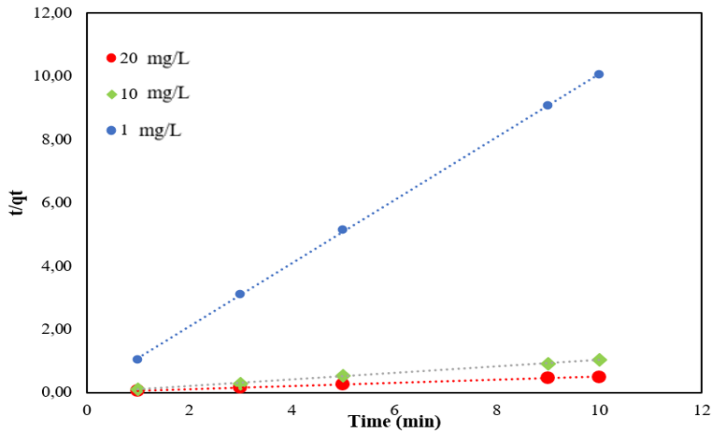

Figure 16. Linearity of the pseudo-second-order kinetic model. Adsorption experiments of As at 1, 10, and 20 mg/L using FeNPs-CR.

The adsorption mechanism of arsenic onto FeNPs-CR can be interpreted by considering the combined contribution of the iron oxide core and the organic functional groups derived from the tangerine peel extract. Although adsorption experiments using the individual pristine components were not conducted, the experimental evidence obtained in this study enables a mechanistic interpretation based on well-established adsorption behavior.

Iron oxide nanoparticles are known to adsorb arsenic primarily through surface complexation mechanisms involving Fe–OH groups, leading to the formation of inner- or outer-sphere Fe–O–As complexes. This mechanism is strongly pH-dependent and typically favors acidic conditions, which is consistent with the enhanced arsenic removal observed at low pH values in this study [54–56].

In contrast, plant-derived organic materials generally exhibit weaker adsorption capacity toward arsenic, dominated by nonspecific electrostatic interactions and physical adsorption through functional

groups such as hydroxyl and carboxyl moieties. While these interactions alone are usually insufficient to achieve high removal efficiencies, they can contribute to surface charge modulation and improved dispersion of iron oxide nanoparticles [54].

The superior adsorption performance of FeNPs-CR compared to what would be expected from individual components can therefore be attributed to a synergistic effect. The organic coating introduces additional functional groups and enhances surface accessibility, while the iron oxide core provides specific adsorption sites capable of forming surface complexes with arsenic species. Consequently, arsenic adsorption onto FeNPs-CR is governed by a combined mechanism involving electrostatic attraction at low pH and surface complexation at iron oxide sites.

3.7. Thermodynamic study

Thermodynamic parameters (Table 2) were determined using adsorption data obtained at different temperatures for As concentrations of 1, 10, and 20 mg/L. These experiments were performed separately from the factorial studies and were designed to evaluate the temperature dependence of As adsorption onto FeNPs-CR.

For the thermodynamic analysis, the changes in enthalpy (ΔH) and entropy (ΔS) were calculated from the slope of the ln Kc versus 1/T plot. The thermodynamic parameters used to evaluate arsenic adsorption onto FeNPs-CR are summarized in Table 2.

Table 2. Thermodynamic parameters of As in FeNPs-CR.

T(K)	In Kc	G (kJ/mol)	H (kJ/mol)	S (J/mol*K)
300	4.49	-11.14	-63.008	174.41
308	3.54	-9.06		
318	2.90	-7.66		

Once these parameters were analyzed, the Langmuir and Freundlich isotherm models were applied based on the experimental data obtained. In this analysis, thermodynamic factors in the liquid phase were considered, including temperature, contact time, and the concentrations of the contaminant and the adsorbent, to identify the optimal conditions that enhance arsenic removal efficiency [57].

The application of the Langmuir and Freundlich isotherm models enables the evaluation of the interactions between FeNPs-CR and arsenic in aqueous systems as a function of key operational parameters, such as contact time, adsorbent dosage, and contaminant concentration. These interactions are governed by a combination of physical and chemical processes, which may occur simultaneously during adsorption.

Furthermore, this analysis is particularly relevant because FeNPs-CR were synthesized through a green synthesis route, contributing to reduced environmental impact while maintaining high arsenic removal efficiency. The use of environmentally friendly synthesis methods therefore represents a promising approach for the development of efficient and sustainable adsorbents for water treatment applications [47,48].

4. Discussion

The synthesis of FeNPs-CR through the coprecipitation method assisted by Citrus reticulata extract yielded a material with structural and surface properties favorable for arsenic removal from

aqueous solutions. The 2:1 molar ratio of Fe(III)/Fe(II) under alkaline conditions (pH 10) promotes the formation of magnetite (Fe_3O_4), a phase recognized for its high surface reactivity and chemical stability. The incorporation of the plant extract played a key role not only as a reducing and stabilizing agent but also as a modifier of surface chemistry. FTIR analyses revealed the presence of functional groups such as –OH and –COOH associated with phenolic compounds and biomolecules from the extract, which contribute to increasing the energetic heterogeneity of the surface. SEM micrographs showed particles ranging from 70 to 300 nm, indicating a certain degree of polydispersity and possible partial aggregation, a phenomenon commonly observed in green synthesis routes, which may nevertheless favor the generation of a broad distribution of active sites [58].

Removal experiments demonstrated efficiencies greater than 99% at an initial concentration of 20 mg/L within short contact times (10–30 min), indicating rapid kinetics dominated by the availability of accessible surface sites. Even at higher concentrations (50, 80, and 120 mg/L), removal efficiency remained above 95%, indicating a strong affinity of the material for arsenic over a wide concentration range. This behavior suggests that the process is not initially limited by intraparticle diffusion but rather by direct interactions at the adsorbent surface. The rapid initial uptake can be attributed to the high density of active functional groups introduced during the green synthesis, which facilitate electrostatic attraction and surface complexation mechanisms.

Isotherm analysis provided key insights into the adsorption mechanism. The Langmuir model showed a poor fit ($R^2 = 0.46$), indicating that the system does not follow an ideal monolayer adsorption behavior on a homogeneous surface, despite the high theoretical qmax value (227.27 mg/g). In contrast, the Freundlich model exhibited an excellent fit ($R^2 = 0.97$), confirming that adsorption occurs on a heterogeneous surface with a distribution of interaction energies. The KF value (23.87 mg/g) supports the high adsorption capacity of the material, while the 1/n parameter (1.089) suggests a favorable process with possible complexity in the adsorbent–adsorbate interaction. This behavior is consistent with the organic functionalization introduced by the plant extract, which generates multiple types of active sites with varying affinities toward arsenic species [59].

The effect of pH confirmed that arsenic speciation and the surface charge of the adsorbent significantly control the process. Under highly acidic conditions (pH 1–3), surface protonation enhances electrostatic attraction toward predominantly anionic arsenic species, resulting in increased removal efficiency. At neutral pH, the observed decrease may be attributed to competition with hydroxide ions and changes in surface potential. Furthermore, the reduction in efficiency at elevated temperatures (35–45 °C) confirms the exothermic nature of the process, suggesting that increasing temperature reduces the stability of adsorbed species on the surface [60]. This behavior indicates that the mechanism includes a significant physical adsorption component, although the high efficiency observed also suggests the contribution of surface chemical interactions.

Overall, the combination of structural characterization, isotherm behavior, pH dependence, and temperature effects indicate that arsenic adsorption onto FeNPs-CR is governed by a heterogeneous and multifactorial mechanism in which electrostatic attraction and surface complexation with active functional groups coexist. The high adsorption capacity, together with the enhanced stability provided by green synthesis, positions FeNPs-CR as a competitive material compared to other iron-based adsorbents reported in the literature. Nevertheless, to consolidate its applicability in real water treatment systems, further evaluation in complex matrices containing competing species, as well as regeneration and long-term stability studies, would be necessary.

5. Conclusions

Based on the characterization results, it was determined that the coprecipitation method using Fe(III) and Fe(II) salts in a 2:1 molar ratio, combined with the addition of 1 mL of *Citrus reticulata* peel extract (75 g of pulverized peel) at pH 10 adjusted with 0.4 M NaOH, provides optimal conditions for the synthesis of FeNPs-CR. FeNPs-CR were successfully characterized using FTIR, UV–Vis spectroscopy, and SEM. The results obtained from these techniques are consistent with other reported data for FeNPs-CR. The synthesized nanoparticles exhibited particle sizes ranging from approximately 70 to 300 nm and displayed characteristic absorption bands and spectral features associated with this type of nanomaterial. Arsenic removal experiments demonstrated that FeNPs-CR achieve removal efficiencies greater than 99% within contact times between 10 and 30 min at an initial As concentration of 20 mg/L. At higher concentrations (50, 80, and 120 mg/L), removal efficiencies remained above 95%, indicating a strong affinity of FeNPs-CR toward arsenic over a wide concentration range.

Temperature and pH were identified as key operational parameters influencing adsorption performance. Higher temperatures (35 and 45 ℃) resulted in decreased removal efficiency, confirming the exothermic nature of the adsorption process. In contrast, adsorption was most effective under acidic conditions, particularly at pH values between 1 and 3, where removal efficiencies were significantly higher than those observed at neutral pH. The use of *Citrus reticulata* peel extract enabled the green synthesis of FeNPs-CR, providing enhanced stability by reducing oxidation and agglomeration of the nanoparticles. The organic components of the extract contribute additional surface functional groups, increasing the effective surface area and the availability of active sites for arsenic adsorption. Overall, the results demonstrate that FeNPs-CR synthesized via an environmentally friendly route exhibit high adsorption efficiency and selectivity toward arsenic. Future studies are recommended to evaluate the performance of FeNPs-CR in natural water samples to assess matrix effects and the influence of competing species, thereby further validating their potential application in practical water treatment systems.

Use of AI tools declaration

The authors declare they have not used Artificial Intelligence (AI) tools in the creation of this article.

Acknowledgments

The authors gratefully acknowledge the financial and institutional support provided by Project DIPI-024 of the Escuela Superior Politécnica de Chimborazo (ESPOCH), entitled “Desarrollo de un tratamiento in situ de relaves mineros para su vertido y recuperación de metales pesados: Aplicación a Zaruma–Ecuador.”

Hugo Sánchez-Moreno: Conceptualization, methodology, formal analysis, investigation, writing–original draft, supervision, project administration; Ingrid Haro-Chafla: Investigation, data curation, validation, writing–review & editing; Juan Lagua-Chango: Methodology, investigation, resources, validation; Benjamín Román-Santos: Formal analysis, software, data curation; Nelly Guananga-Díaz: Investigation, visualization, validation; David Espín-García: Resources, supervision, writing–review & editing; Lis Peñafiel-Guevara: Investigation, data curation, visualization; Israel Heredia-Moreno: Supervision, funding acquisition, writing–review & editing. All authors have read and approved the final version of the manuscript for publication.

Conflict of interest

All authors declare no conflicts of interest in this paper.

References

1. Sharma VK, Sohn M (2009) *Aquatic arsenic: Toxicity, speciation, transformations, and remediation*, Elsevier. https://doi.org/10.1016/j.envint.2009.01.005
2. A. Heredia, Avila JG, Vinuesa A, et al. (2019) Compared arsenic removal from aqueous solutions by synthetic mixed oxides and modified natural zeolites. *Adsorption* 25: 1425–1436. 10.1007/s10450-019-00109-2
3. M. Khute, Sharma S, Patel KS, et al. (2024) Contamination, speciation, and health risk assessment of arsenic in leafy vegetables in Ambagarh Chowki (India), *Anal Sci* 40: 1553–5160. https://doi.org/10.1007/s44211-024-00579-7
4. Mohsenzadeh A, Poorkhalil A, Tabesh H, et al. (2025) Arsenic removal from water using iron-modified nanoclinoptilolite: Inspired by iron plaque mechanisms in rice roots. *Int J Environ Sci Te* 22: 11827–22842. https://doi.org/10.1007/s13762-025-06604-0
5. O. Diaz, Arcos R, Tapia Y, et al. (2015) Estimation of arsenic intake from drinking water and food (raw and cooked) in a rural village of Northern Chile. Urine as a biomarker of recent exposure. *Int J Env Res Pub He* 12: 5614–5633. https://doi.org/10.3390/ijerph120505614
6. M. Faria, Arcos R, Tapia Y, et al. (2023) Arsenic in mining areas: Environmental contamination routes. *Int J Env Res Pub He* 20: 4291. https://doi.org/10.3390/ijerph20054291
7. ALSamman MT, Sotelo S, Sánchez J, et al. (2023) Arsenic oxidation and its subsequent removal from water: An overview. *Sep Purif Technol* 309: 123055. https://doi.org/10.1016/j.seppur.2022.123055
8. Ji S, Fattah TMA (2025) Advancing arsenic water treatment using UiO-66 and its functionalized metal–organic framework analogs. *Nanomaterials* 15: 1621. https://doi.org/10.3390/nano15211621
9. Kumari S, Raturi S, Kulshrestha S, et al. (2023) A comprehensive review on various techniques used for synthesizing nanoparticles. *J Mater Res Technol* 27: 1739–1763. https://doi.org/10.1016/j.jmrt.2023.09.291
10. Raut SS, Singh R, Lekhak UM (2024) Naturally occurring nanoparticles (NONPs): A review. *Next Sustain* 3: 100037. https://doi.org/10.1016/j.nxsust.2024.100037
11. Rathod S, Preetam S, Pandey C, et al. (2024) Exploring synthesis and applications of green nanoparticles and the role of nanotechnology in wastewater treatment. *Biotechnol Rep* 41. https://doi.org/10.1016/j.btre.2024.e00830
12. Niculescu AG, Chircov C, Grumezescu AM (2022) Magnetite nanoparticles: Synthesis methods—A comparative review. *Methods* 199: 16–27. https://doi.org/10.1016/j.ymeth.2021.04.018
13. Yew YP, Shameli K, Miyake M, et al. (2009) Green biosynthesis of superparamagnetic magnetite Fe_3O_4 nanoparticles and biomedical applications in targeted anticancer drug delivery system: A review. *Arab J Chem* 13: 2287–2308. https://doi.org/10.1016/j.arabjc.2018.04.013
14. Eigenfeld M, Reindl M, Sun X, et al. (2024) Exploring multi-parameter effects on iron oxide nanoparticle synthesis by SAXS analysis. *Crystals* 14: 961. https://doi.org/10.3390/cryst14110961
15. Kumar V, Kaushik NK, Tiwari SK, et al. (2023) Green synthesis of iron nanoparticles: Sources and multifarious biotechnological applications. *Int J Biol Macromol* 253: 127017. https://doi.org/10.1016/j.ijbiomac.2023.127017
16. Haider FU, Zulfiqar U, ul Ain N, et al. (2024) Harnessing plant extracts for eco-friendly synthesis of iron nanoparticle (Fe-NPs): Characterization and their potential applications for ameliorating environmental pollutants. *Ecotox Environ Safe* 281: 116620. https://doi.org/10.1016/j.ecoenv.2024.116620

17. Bertolo MRV, Pereira TS, dos Santos FV, et al. (2025) Citrus wastes as sustainable materials for active and intelligent food packaging: Current advances. *Compr Rev Food Sci F* 24: e70144. https://doi.org/10.1111/1541-4337.70144
18. Cho Y, Hwang S, Ninh PTT, et al. (2026) Sustainable valorization of mandarin peel waste into multifunctional cellulose/pectin/PVA films with superior mechanical and UV-blocking performance. *RSC Sustain* 4: 289–303. https://doi.org/10.1039/D5SU00465A
19. Zhu M, Liu X, Xiang D, et al. (2024) The design of high-efficient MOFs for selective Ag(I) capture: DFT calculations and practical applications. *J Hazard Mater* 476: 135204. https://doi.org/10.1016/j.jhazmat.2024.135204
20. Doğan M, Sabaz P, Bicil Z, et al. (2020) Activated carbon synthesis from tangerine peel and its use in hydrogen storage. *J Energy Inst* 93: 2176–2185. https://doi.org/10.1016/j.joei.2020.05.011
21. Liu X, Lu J, Fang X, et al. (2022) Complexation modelling and oxidation mechanism of organic pollutants in cotton pulp black liquor during iron salt precipitation and electrochemical treatment. *Chemosphere* 308: 136374. https://doi.org/10.1016/j.chemosphere.2022.136374
22. Gorohovs M, Dekhtyar Y (2025) Surface functionalization of nanoparticles for enhanced electrostatic adsorption of biomolecules. *Molecules* 30: 3206. https://doi.org/10.3390/molecules30153206
23. Eker F, Akdaşçi E, Duman H, et al. (2025) Green synthesis of silver nanoparticles using plant extracts: A comprehensive review of physicochemical properties and multifunctional applications. *Int J Mol Sci* 26: 6222. https://doi.org/10.3390/ijms26136222
24. Pérez LV, Sánchez HJ, Cando VM, et al. (2022) Fortification of low-fat yogurt with melluco flour (ullucus tuberosus): Physicochemical and rheological effects. *African J Food Agri Nutr Dev* 22: 22041–22058. https://doi.org/10.18697/ajfand.115.20870
25. Kusumahastuti DKA, Gintu AR (2025) Green nanotechnology: silver nanoparticle synthesis via brewed coffee grounds extract. *J Incl Phenom Macro* 105: 241–247. https://doi.org/10.1007/s10847-025-01294-0
26. Assefa H, Singh S, Shehata N, et al. (2024) Green synthesis and characterization of CuO/PANI nanocomposite for efficient Pb (II) adsorption from contaminated water. *Sci Rep* 14: 30972. https://doi.org/10.1038/s41598-024-81970-2
27. Li H, Song W, Li Z, et al. (2025) Adsorption of As(III) to schwertmannite: Impact factors and phase transformation. *Environ Geochem Hlth* 47: 122. https://doi.org/10.1007/s10653-025-02433-9
28. Salem ANM, Ahmed MA, El-Shahat MF (2016) Selective adsorption of amaranth dye on Fe3O4/MgO nanoparticles. *J Mol Liq* 219: 780–788. https://doi.org/10.1016/j.molliq.2016.03.084
29. Matić P, Ukić S, Jakobek L (2024) Adsorption of procyanidins B1 and B2 onto β-Glucan: Adsorption isotherms and thermodynamics. *Adsorption* 30: 1303–1313. https://doi.org/10.1007/s10450-024-00503-5
30. Ajitha B, Reddy YAK, Reddy PS (2015) Green synthesis and characterization of silver nanoparticles using Lantana camara leaf extract. *Mat Sci Eng C* 49: 373–381. https://doi.org/10.1016/j.msec.2015.01.035
31. Akhtar MS, Fiaz S, Aslam S, et al. (2024) Green synthesis of magnetite iron oxide nanoparticles using Azadirachta indica leaf extract loaded on reduced graphene oxide and degradation of methylene blue. *Sci Rep* 14: 18172. https://doi.org/10.1038/s41598-024-69184-y
32. Pillai P, Kakadiya N, Timaniya Z, et al. (2019) *Removal of arsenic using iron oxide amended with rice husk nanoparticles from aqueous solution*, In: Materials Today: Proceedings, Elsevier, 830–835. https://doi.org/10.1016/j.matpr.2019.12.307
33. Osorio FO, Badillo ENV, Rondón DGE, et al. (2023) Drug loading comparison of commercial ibuprofen on magnetite nanoparticles surface by UV–Vis spectrophotometry and acid-alkali titration by a factorial design of experiments. *OpenNano* 14: 100193. https://doi.org/10.1016/j.onano.2023.100193

34. Urquizo IAF, Casillas PG, González CC (2017) Development of magnetic nanoparticles Fe+32 X+21O4 (X= Fe, Co y Ni) coated by amino silane. *Rev Mex Ing Biom* 38: 402–411. https://doi.org/10.17488/RMIB.38.1.36
35. Cruz JI, Colina JS, Moreno HS, et al. (2024) Copper Nanoparticles Enhance Bactericidal Activity of 70% Ethanol Against Multidrug-Resistant Serratia marcescens. *Bionatura J* 1: 1–11. https://doi.org/10.70099/BJ/2024.01.02.18
36. Ehrampoush MH, Miria M, Salmani MH, et al. (2015) Cadmium removal from aqueous solution by green synthesis iron oxide nanoparticles with tangerine peel extract. *J Environ Health Sci* 13. https://doi.org/10.1186/s40201-015-0237-4
37. Deepak FL, López MB, Argibay EC, et al. (2015) A systematic study of the structural and magnetic properties of Mn-, Co-, and Ni-doped colloidal magnetite nanoparticles. *J Phys Chem C* 119: 11947–11957. https://doi.org/10.1021/acs.jpcc.5b01575
38. Villegas VAR, Ramírez JIDL, Guevara EH, et al. (2020) Synthesis and characterization of magnetite nanoparticles for photocatalysis of nitrobenzene. *J Saudi Chem Soc* 24: 223–235. https://doi.org/10.1016/j.jscs.2019.12.004
39. Guerrini L, Puebla RAA, Perez NP (2018) Surface modifications of nanoparticles for stability in biological fluids. *Materials* 11: 1154. https://doi.org/10.3390/ma11071154
40. Serantes D, Baldomir D (2021) Nanoparticle size threshold for magnetic agglomeration and associated hyperthermia performance. *Nanomaterials* 11: 2786. https://doi.org/10.3390/nano11112786
41. Vikesland PJ, Rebodos RL, Bottero JY, et al. (2025) Aggregation and sedimentation of magnetite nanoparticle clusters. *Environ Sci Nano* 3: 567–577. https://doi.org/10.1039/C5EN00155B
42. Sentis MPL, Feltin N, Lambeng N, et al. (2024) Investigation of nanoparticle dispersibility and stability based on TiO_2 analysis by SMLS, DLS, and SEM. *J Nanopart Res* 26: 55. https://doi.org/10.1007/s11051-024-05959-8
43. Stetefeld J, McKenna SA, Patel TR (2016) Dynamic light scattering: A practical guide and applications in biomedical sciences. *Biophys Rev* 8: 409–427. https://doi.org/10.1007/s12551-016-0218-6
44. Din SU, Mahmood T, Naeem A, et al. (2019) Detailed kinetics study of arsenate adsorption by a sequentially precipitated binary oxide of iron and silicon. *Environ Technol* 40: 261–269. https://doi.org/10.1080/09593330.2017.1385649
45. Sharma G, Vermaa Y, Lai CW, et al. (2025) Biochar and biosorbents derived from biomass for arsenic remediation. *Heliyon* 10: e36288. https://doi.org/10.1016/j.heliyon.2024.e36288
46. Moreno HS, Altamirano K, Escobar S, et al. (2025) Removal of lead (II) from aqueous solutions using iron nanoparticles synthesized from watermelon peel extract. *AIMS Environ Sci* 12: 653–682. https://doi.org/10.3934/environsci.2025029
47. Moreno HS, Malca J, Zambrano M, et al. (2025) Green synthesis of iron nanoparticles from Pouteria caimito: An effective adsorbent for mercury (Hg) in aqueous solutions. *Results Mater* 28: 100784. https://doi.org/10.1016/j.rinma.2025.100784
48. McGeogh M, Annath H, Mangwandi C (2024) Turning teawaste particles into magnetic bio-sorbents particles for arsenic removal from wastewater: Isotherm and kinetic studies. *Particuology* 87: 179–193. https://doi.org/10.1016/j.partic.2023.08.003
49. Chen HH, Chang YC, Wei WK, et al. (2025) Treatment of arsenic-contaminated groundwater with a novel iron oxide/carbon composite as the adsorbent. *Water Air Soil Pollut* 235. https://doi.org/10.1007/s11270-024-07522-6
50. Yohai L, Uheida A, Pellice S (2024) Nanoparticle-nanofiber synergistic matrix for highly effective arsenic adsorption: material design and performance evaluation. *J Solgel Sci Technol* 109: 385–399. https://doi.org/10.1007/s10971-023-06277-6

51. Moreno HS, Rodríguez LG, Moreno CR (2025) Natural cellulose fibers (Agave Americana L. ASPARAGACEAE) impregnated with magnetite nanoparticles as a novel adsorbent of mercury (Hg) in aqueous solutions. *Adsorption* 31. https://doi.org/10.1007/s10450-024-00577-1
52. Hussein EB, Rasheed FA (2025) Enhanced amoxicillin adsorption from wastewater using KOH-modified Iraqi Silica Sand: Characterization, kinetics, and thermodynamics. *Int J Environ Res* 19. https://doi.org/10.1007/s41742-025-00805-8
53. Moreno HS, Rodríguez LG, Moreno CR (2025) Natural cellulose fibers from Agave Americana L. ASPARAGACEAE as an effective adsorbent for mercury in aqueous solutions. *Adsorption* 31. https://doi.org/10.1007/s10450-024-00590-4
54. Gong S, Yang J, Zhou W, et al. (2023) Fe-containing materials for inorganic/organic arsenic removal from water: A review of current status and future prospects. *J Clean Prod* 428: 139533. https://doi.org/10.1016/j.jclepro.2023.139533
55. Boruah H, Tyagi N, Gupta SK, et al. (2025) Understanding the adsorption of iron oxide nanomaterials in magnetite and bimetallic form for the removal of arsenic from water. *Front Environ Sci* 11. https://doi.org/10.3389/fenvs.2023.1104320
56. Apaza LDV, Collantes AC, Acosta RS, et al. (2024) Aqueous-medium Arsenic(V) removal using iron oxide-coated ignimbrite *Water* 17: 53. https://doi.org/10.3390/w17010053
57. Mohanta J, Dey B, Dey S (2024) Magnetic cobalt and nickel oxide nanoparticles for excellent arsenic withdrawal from water. *Chem Pap* 78: 4841–4856. https://doi.org/10.1007/s11696-024-03433-2
58. Elgoud EMA, Elhamid AIA, Aly HF (2024) Adsorption behavior of Mo(VI) from aqueous solutions using tungstate-modified magnetic nanoparticle. *Environ Sci Pollut R* 31: 18900–18915. https://doi.org/10.1007/s11356-024-32251-y
59. Gafaru IA, Cobbina SJ, Michael K (2025) Green-synthesized magnetic iron oxide nanoparticles for the adsorptive removal of CD^{2+} and PB^{2+} from aqueous solution. *DIWA* 5. https://doi.org/10.1007/s43832-025-00285-z
60. Rorissa GL, Tesema EA, D.M. RP, et al. (2025) Removal of methylene blue dye from textile industry wastewater using green synthesized Teff straw assisted ZnO nanoparticle. *Sci Rep* 15: 26230. https://doi.org/10.1038/s41598-025-11746-9

AIMS Press